A New Augmented L1 Adaptive Control for Wheel-Legged Robots: Design and Experiments

Fahad Raza, Ahmed Chemori, Mitsuhiro Hayashibe

2022 American Control Conference (ACC)
Atlanta, USA, June 8-10, 2022

A New Augmented $\mathcal{L}_1$ Adaptive Control for Wheel-Legged Robots: Design and Experiments

Fahad Raza[1], Ahmed Chemori[2] Senior Member, IEEE
and Mitsuhiro Hayashibe[1] Senior Member, IEEE

***Abstract*— This paper proposes the augmentation of an $\mathcal{L}_1$ adaptive controller with a feedback Linear Quadratic Regulator (LQR) to control a wheel-legged biped robot. The performance of linearized model-based controllers, such as LQR, depends on the accurate knowledge of model parameters, a priori information about input and output disturbances, and other unforeseen conditions. We propose a hybrid scheme where an $\mathcal{L}_1$ adaptive controller is combined with LQR to compensate for matched uncertainties and other disturbances related to the environment change such as friction conditions of the floor. The proposed control scheme is able to keep the robot stable under model uncertainties and external disturbances through a series of validation scenarios including simulations and real-time experiments.**

I. INTRODUCTION

The high maneuverability, speed, and agility of self-balancing wheel-legged robots compared to the legged humanoid robots come in exchange for instability and challenging control system design. Due to a small footprint and a tall body, these robots are well suited and even desired for indoor settings such as restaurants, banks, homes, hotels, etc. However, the robust self-balancing of wheel-legged robots remains the most challenging aspect for deploying these robots in the real world. Most of these applications require a robot that may carry an object from one place to other for automated delivery, or the human guidance service by moving on different floor conditions. These practical requirements further enhance the difficulty in the control problem as the unknown payload incorporates model uncertainty, and the unknown floor friction also creates the need for environmental adaptation.

The safety-critical nature of these systems requires a robust control system design for all practical purposes, and hence gained a significant interest among the control and robotics communities in recent years.

A. Background

In the literature, wheeled inverted pendulum (WIP) robots are divided into two categories, namely with legs also known as wheel-legged robots and without legs. Earlier works on WIP robots were mostly focused on the version without legs. Yuta *et al.* proposed pitch and trajectory control of a WIP robot called Yamabico Kurara and successfully separated its steering control from balancing and translational motion [1] [2]. Tani *et al.* attempted cooperative object transportation using an unstable WIP robot and a human [3]. A control system was built to estimate the external force and exert the required force to maintain the robot in a balanced state.

A team from EPFL developed a WIP robot called JOE [4]. They implemented two decoupled schemes to control its orientation and translational motion along with balancing. In another important study, Agrawal and his team produced partial feedback linearization of a WIP robot while considering its nonholonmic constraints [5] [6]. Takahashi *et al.* introduced an assistant robot with wheeled inverted pendulum mechanism capable of various tasks such as standing, sitting, as well as object picking [7] [8]. A linear quadratic regulator (LQR) was devised and applied for its motion control.

More recently, Boston Dynamics announced its first wheel-legged robot named Handle that can be used as a pick and place robot in industrial warehouses [9]. Also a team from Harbin Institute of technology in China designed a hose-less hydraulic wheel-legged robot able to improve the overall reliability of the hydraulic actuator system [10].

A team from ETH, Zurich also developed a wheel-legged robot called Ascento [11] [12]. The control scheme includes a whole-body controller that incorporates rolling constraints for better performance against curves and an LQR used for the pitch control. Caporale *et al.* proposed a computed torque control law to stabilize a wheeled humanoid robot [13].

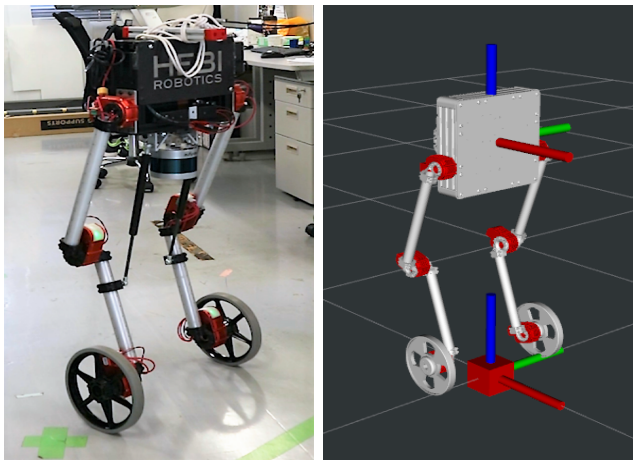

(a) Real robot. (b) 3D model in ROS Rviz.

Fig. 1: View of the Igor wheel-legged robot.

[1]F. Raza and M. Hayashibe are with Department of Robotics, Graduate School of Engineering, Tohoku University, Sendai 980-8579 Japan (e-mail: fahadraza@dc.tohoku.ac.jp; hayashibe@tohoku.ac.jp).

[2]A. Chemori is with the LIRMM, CNRS, University of Montpellier, 34095 Montpellier, France (e-mail: ahmed.chemori@lirmm.fr).

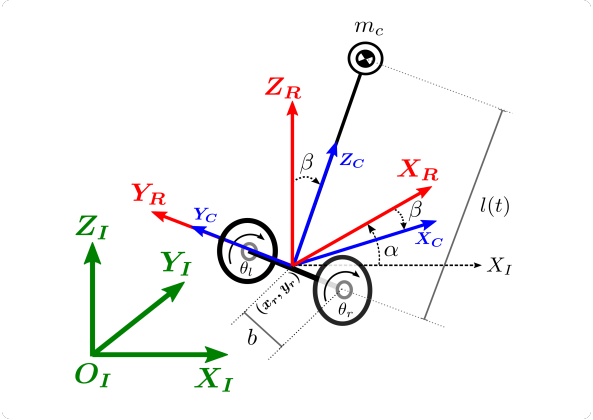

Fig. 2: Model of the robot with generalized coordinates.

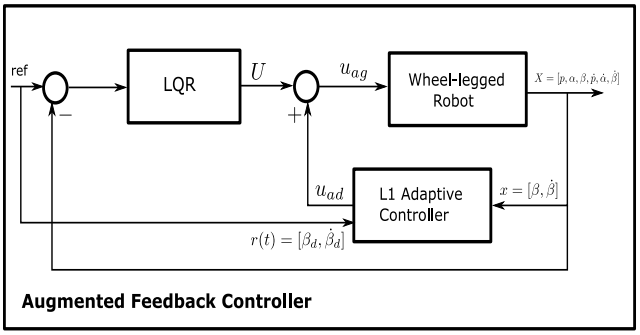

Fig. 3: Structure of the proposed augmented $\mathcal{L}_1$ adaptive controller.

Machine learning techniques are also getting attention recently for balancing and control of wheel-legged robots. In a very recent study, Jiang *et al.* proposed a novel data-driven value iteration algorithm that generates a balancing controller for a wheel-legged robot with a small amount of data [14]. Model learning of a two-wheeled robot where a simulation model is learned first and then the difference model to reduce the sim-to-real gap has also been reported [15]. Further studies also proposed nonlinear sliding-mode controller, optimization based whole-body controller, and nonlinear optimal control for WIP robots [16] [17] [18] [19].

B. Motivation

It is clear from the previous discussion that both linear and nonlinear motion controllers have been designed to balance and control WIP robots. Commonly used model-based controllers depend on system parameters which may change over time, and other assumptions to simplify the system for modeling purposes. Moreover, linear motion controllers such as LQR are mainly based on linearized models of the system and hence relevant for only a small region around the operating point. We believe an adaptive control mechanism is essential for the wheel-legged system under the assumed circumstances. Accordingly, we propose a new control scheme based on the combination of an LQR feedback controller and an $\mathcal{L}_1$ adaptive controller to compensate for modeling errors, external disturbances, and other eventual uncertainties. To the best of the authors' knowledge, it is the first time that an adaptive control scheme has been proposed for a wheel-legged robot with experimental validation on a real system.

II. Model of The Wheel-Legged Robot

This section provides the mathematical modeling of the wheel-legged robot named Igor illustrated in Fig. 1. The robot has three degrees of freedom (DoF); including the translational motion, the heading angle or orientation, and the pitch angle. Three reference frames Σ_I, Σ_R, and Σ_C are considered to completely describe the robot in the world frame as illustrated in Fig. 2. Σ_I is the inertial frame attached to the ground, Σ_R is the robot base frame, and Σ_C is the Center of Mass (CoM) frame. Further, the origins of Σ_R and Σ_C coincide.

The pitch angle (β) is defined as the angle between Z_R and Z_C, representing Z-axes of Σ_R and Σ_C, respectively. The heading angle (α) represents the angle between X_R and X_I axes of Σ_R and Σ_I frames. Six parameters are used to derive the dynamics of the robot in the inertial frame; ${}_Ix_r$ and ${}_Iy_r$ define the robot base location, θ_r and θ_l denote the right wheel and left wheel displacements, respectively, and α, β are the yaw and pitch displacements of the robot.

The nonlinear dynamic model of the robot is then obtained using Euler-Lagrange method as detailed in [20] [21]. The renowned manipulator equation of the robot with nonholonomic constraints due to its differential drive is as follows

$$M(q)\ddot{q} + V\dot{q} + H(q,\dot{q}) + G = E\tau + J(q)^T\lambda, \quad (1)$$

where $M(q) \in \mathbb{R}^{6\times6}$ is the inertia matrix, $V \in \mathbb{R}^{6\times6}$ is a matrix of viscous coefficients, $H(q,\dot{q}) \in \mathbb{R}^6$ includes centrifugal and coriolis terms, $G \in \mathbb{R}^6$ is the gravity vector, $E \in \mathbb{R}^{6\times2}$ is the torque selection matrix, $\tau \in \mathbb{R}^2$ is the control input torque vector, $J(q)$ defines nonholonomic and holonomic constraints of the robot, λ is Lagrange multiplier, and vector $q = [{}_Ix_r \ {}_Iy_r \ \alpha \ \beta \ \theta_r \ \theta_l]^T$ represents the generalized coordinates.

Finally, after removing the Lagrange multiplier λ and linearizing the model around its equilibrium point $\beta = 0$, we get the reduced-order linear model in the state-space form as follows

$$\begin{aligned} \dot{X} &= AX + BU \\ Y &= CX + DU, \end{aligned} \quad (2)$$

where $X = [p \ \alpha \ \beta \ \dot{p} \ \dot{\alpha} \ \dot{\beta}]^T$ is the state vector, and $p = {}_Ix_r\cos(\alpha) + {}_Iy_r\sin(\alpha)$ is the translational position of the robot. $Y \in \mathbb{R}^6$ represents the output vector of the system, and $U \in \mathbb{R}^2$ is the control input. The matrices A, B, C, and D are respectively called state, input, output, and feedforward matrices.

III. Proposed Control Scheme

This section introduces the proposed control method to stabilize the wheel-legged robot which is inherently unstable in nature. The proposed augmented $\mathcal{L}_1$ adaptive control

framework is represented in Fig. 3.

A. Linear Quadratic Regulator (LQR)

A linear quadratic regulator is a full state feedback optimal controller that places the poles of the closed-loop system to minimize the following quadratic cost function

$$J_{lqr} = \int_0^\infty [X(t)^T Q X(t) + U(t)^T R U(t)]\ dt,$$

where Q and R define weights for the system states and the control inputs, respectively.
The state feedback control law that minimizes the above cost function is

$$U = ref - K_{lqr} X, \tag{3}$$

here ref represents the reference signal.
The state feedback gain K_{lqr} is given by

$$K_{lqr} = R^{-1} B^T P,$$

where P is obtained by solving the following algebraic Riccati equation (ARE)

$$A^T P + PA - PBR^{-1}B^T P + Q = 0 \tag{4}$$

The matrices A and B are obtained using the parameters of the wheel-legged robot summarized in TABLE I, while Q and R are tuned with a trial-and-error method to get satisfying performance in the real-time system. After obtaining the matrices, we obtained the following K_{lqr} value by utilizing the pole placement technique,

$$K_{lqr} = \begin{bmatrix} -2.8284 & 1.4142 & -19.4797 & -4.8849 & 0.4032 & -4.7839 \\ -2.8284 & -1.4142 & -19.4797 & -4.8849 & -0.4032 & -4.7839 \end{bmatrix}.$$

B. Background on $\mathcal{L}_1$ Adaptive Control

This section describes the design of an adaptive control system for the pitch angle (β) stabilization of the wheel-legged robot. For a safety-critical system like a self-balancing robot, keeping it in the upright position is of utmost importance to avoid any accident, and damage of the robot and its environment. Accordingly, we introduce the method where an $\mathcal{L}_1$ adaptive controller is augmented with an LQR controller in order to keep the robot stable in unforeseen circumstances.
The decoupling between adaptation and robustness ensured by the $\mathcal{L}_1$ adaptive control architecture makes it an ideal adaptive controller for real-time applications. High adaptation gains for achieving fast convergence can be used without introducing a high frequency signal in the control input. The control scheme proposed in this section is based on the $\mathcal{L}_1$ adaptive control theory for systems with time-varying parameters and disturbances along with uncertain system input gain [22].
The $\mathcal{L}_1$ adaptive control consists of an adaptation and a prediction stage as illustrated in Fig. 4. The adaptation phase is used to predict the unknown and/or time-varying parameters and other uncertainties including external disturbances, whereas the prediction stage is used to get the ideal required performance of the system. Furthermore, a low pass filter is

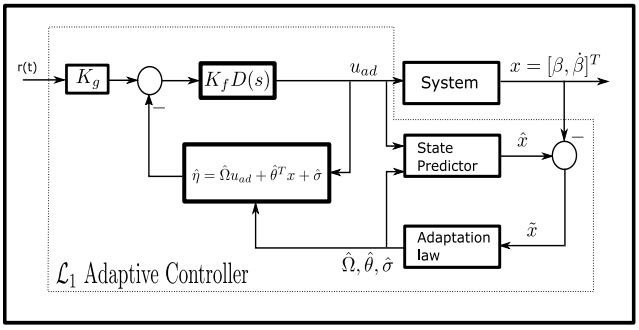

Fig. 4: Block diagram of $\mathcal{L}_1$ Adaptive Control.

incorporated in the closed-loop to remove high frequencies from the control signal that may occur due to high adaptation gains.
Let us consider the inverted pendulum model that is extracted from (1) in the form

$$\begin{aligned} \dot{x}(t) &= A_p x(t) + B_p(\Omega u_{ad}(t) + \theta^T(t) x(t) + \sigma(t)), \\ y(t) &= C_p x(t) \end{aligned} \tag{5}$$

where A_p is the known $\mathbb{R}^{2\times 2}$ matrix that describes the linear dynamics of the inverted pendulum, $x(t) = [\beta\ \dot{\beta}]^T \in \mathbb{R}^2$ is the state vector, $B_p \in \mathbb{R}^2$ and $C_p \in \mathbb{R}^{2\times 2}$ known matrices, $\theta(t) \in \mathbb{R}^2$ vector of time-varying unknown parameters, $\sigma(t) \in \mathbb{R}$ models eventual disturbances and unmodeled dynamics, $\Omega \in \mathbb{R}$ is an unknown positive constant and $u_{ad}(t) \in \mathbb{R}$ is the adaptive control input.

1) State Predictor: To develop a full-state feedback controller so that the system output $y(t)$ tracks the reference signal $r(t)$, we consider a state predictor of the form

$$\begin{aligned} \dot{\hat{x}}(t) &= A_m \hat{x}(t) + B_p(\hat{\Omega}(t) u_{ad}(t) + \hat{\theta}^T x(t) + \hat{\sigma}(t)), \\ \hat{y}(t) &= C_p \hat{x}(t) \end{aligned} \tag{6}$$

here $A_m = A_p - B_p K_m \in \mathbb{R}^{2\times 2}$ is a known Hurwitz matrix, whereas $\hat{\theta}$, $\hat{\sigma}$, and $\hat{\Omega}$ are the estimates of θ, σ, and Ω, respectively.

2) Adaptation Law: The estimations of the parameters are governed by the following projection-based adaptive laws

$$\begin{aligned} \dot{\hat{\theta}}(t) &= Proj(\hat{\theta}(t), -\Gamma_\theta \tilde{x}^T(t) P_a B_p x(t)),\ \hat{\theta}(0) = \hat{\theta}_0, \\ \dot{\hat{\sigma}}(t) &= Proj(\hat{\sigma}(t), -\Gamma_\sigma \tilde{x}^T(t) P_a B_p),\ \hat{\sigma}(0) = \hat{\sigma}_0, \\ \dot{\hat{\Omega}}(t) &= Proj(\hat{\Omega}(t), -\Gamma_\Omega \tilde{x}^T(t) P_a B_p u_{ad}(t)),\ \hat{\Omega}(0) = 1, \end{aligned} \tag{7}$$

where $\Gamma_\Omega > 0$, $\Gamma_\sigma > 0$, and $\Gamma_\theta > 0$ are the adaptation gains, $\tilde{x}(t) = \hat{x}(t) - x(t)$ is the prediction error, and $P_a = P_a^T > 0$ is the solution of Lyapunov equation $A_m^T P_a + P_a A_m = -Q_a$ for an arbitrary symmetric matrix $Q_a = Q_a^T > 0$.

3) Projection Operator: A projection operator is used for updating the parameters $\hat{\theta}, \hat{\sigma}$, and $\hat{\Omega}$ smoothly and confining them within the required set [23]. The algorithm of the projection operator $Proj(z, \phi)$, used in (7) for a parameter z, is described as follows,

Algorithm **:** Projection Operator

Inputs **:** ϵ, z, ϕ, z_{max}, z_{min}
1 : compute $f_d = (z_{max} - z_{min})^2$;
2 : compute $f_z = \frac{-4*(z_{min}-z)*(z_{max}-z)}{\epsilon * f_d}$;
3 : compute $f_{\dot{z}} = \frac{4*(z_{min}+z_{max}-2*z)}{\epsilon * f_d}$;
4 : define $output = \phi$;
5 : ***if*** $(f_z <= 0 \; and \; f_{\dot{z}} * \phi < 0)$ ***then***
$output = \phi * (f_z + 1)$;
6 : ***return*** output;

here, $0 < \epsilon < 1$ is a constant that sets the steepness of the curve. z_{max} and z_{min} are respectively the maximum and minimum values delimiting the admissible range of the parameter z.

4) Adaptive Control Law: According to the block diagram of Fig. 4, the adaptive control input u_{ad} for the inverted pendulum system (5) is given in Laplace domain as follows;

$$u_{ad}(s) = -K_f D(s)\big(\hat{\eta}(s) - K_g r(s)\big), \tag{8}$$

where K_g is the feedforward gain, $r(s) = [\beta_d, \dot{\beta}_d]^T$ is the reference signal, $K_f > 0$ is the feedback gain, and $D(s)$ is a strictly proper transfer function such that

$$C(s) = \frac{\Omega K_f D(s)}{1 + \Omega K_f D(s)}, \tag{9}$$

is strictly proper stable transfer function and DC gain $C(0) = 1$. Furthermore,

$$\hat{\eta}(t) = \hat{\Omega} u_{ad}(t) + \hat{\theta}^T(t) x(t) + \hat{\sigma}(t).$$

To ensure the stability of the resulting closed-loop system, the design of the feedback gain K_f and the low-pass filter $D(s)$ should satisfy the following $\mathcal{L}_1$-norm condition

$$\|G(s)\|_{\mathcal{L}_1} L < 1, \tag{10}$$

where $G(s) = H(s)\big(1 - C(s)\big)$, $H(s) = \big(s\mathbb{I} - A_m\big)^{-1} B_p$, and $L = \max_{\theta \in \Theta} \|\theta\|_1$, here Θ is a known convex compact set. The reader is encouraged to refer to [22] for detailed proofs of stability and performance analysis.

IV. Simulation Results

This section provides an overview of the simulation setup used in this study as well as the corresponding obtained results. The wheel-legged robot Igor was defined in the Unified Robotic Description Format (URDF) and simulated in Gazebo simulator using the Robotic Operatic System (ROS). We used C++ programming language to implement the proposed motion control algorithm for better portability and efficiency. The control loop runs at a frequency of 500Hz. The nominal parameters of the system are summarized in TABLE I. To validate the proposed augmented adaptive control scheme qualitatively as well as quantitatively, we conducted two different tests and results are shown in Fig. 5. The main motivation behind these scenarios is to compare the input torques of both controllers, and the pitch angle (β) and pitch rate ($\dot{\beta}$) subject to external disturbances and model uncertainties.

TABLE I: Dynamic parameters of the robot.

Parameters	**Description**	**Value**	**Units**
m_c	Robot body mass.	7.5	Kg
m_w	Robot wheel mass.	0.35	Kg
l	Distance of the CoM from the origin of Σ_R.	0.5914	m
r_w	Wheel radius.	0.1016	m
c_r, c_l	Right wheel and left wheel viscosity coefficients.	0.17	$\frac{N.m}{(rad/sec)}$

In the first scenario, we used the nominal parameters of the robot and compare the augmented control scheme against the model-based LQR. The obtained results from this simulation are depicted in Fig. 5a. We applied a linear force of $20N$ on the robot body at $t = 10s$ for a duration of $1s$. The given plots clearly indicate that the augmented controller keeps the pitch angle (β) and rate ($\dot{\beta}$) smaller than those of the LQR. Furthermore, the settling time of the pitch angle for the proposed controller is about $2.5s$ against $6s$ for LQR.

In the second scenario, to introduce a modeling uncertainty we propose to change the value of the viscous friction coefficient of the wheel actuators from its nominal value $c_r = c_l = 0.17$ to $c_r = c_l = 0.34$ (i.e. $+100\%$). We know that determining these friction coefficients in the real world is near impossible as they change over time due to abrasion and other factors. In case of the model-based LQR as shown in Fig. 5b, it is evident that the impact of inaccurate friction coefficients can be highly risky for a self-balancing robot as it could not recover from the translational push of $20N$. On the other hand, the proposed augmented controller successfully kept the robot around its vertical upright position.

TABLE II summarizes the quantitative difference between the LQR and the proposed augmented controller in different settings. By integrating the torques over time, which is also known as angular impulse, we found that in the nominal case, it is 6.3441 N.m.s against 3.6355 N.m.s for the LQR and the proposed augmented controller, respectively. It is clear that the augmented controller uses upto 42.7% less torque and hence less energy than the LQR in keeping the robot balanced in the nominal case. Besides it is worth to note that the proposed augmented control scheme can endure a linear push of up to $30N$ i.e. 50% more force than the maximum of $20N$ for the LQR.

V. Real-Time Experiments And Results

For the real-time control of the Igor robot, we used ROS with C++ to run the motion control algorithms. The control loop runs on an intel core i7 microprocessor at a frequency of 500Hz and the torque commands are transmitted to the robot actuators through a wifi connection. Besides, for the robot localization we used an extended kalman filter (EKF) to filter and fuse the data from multiple IMUs and the wheel

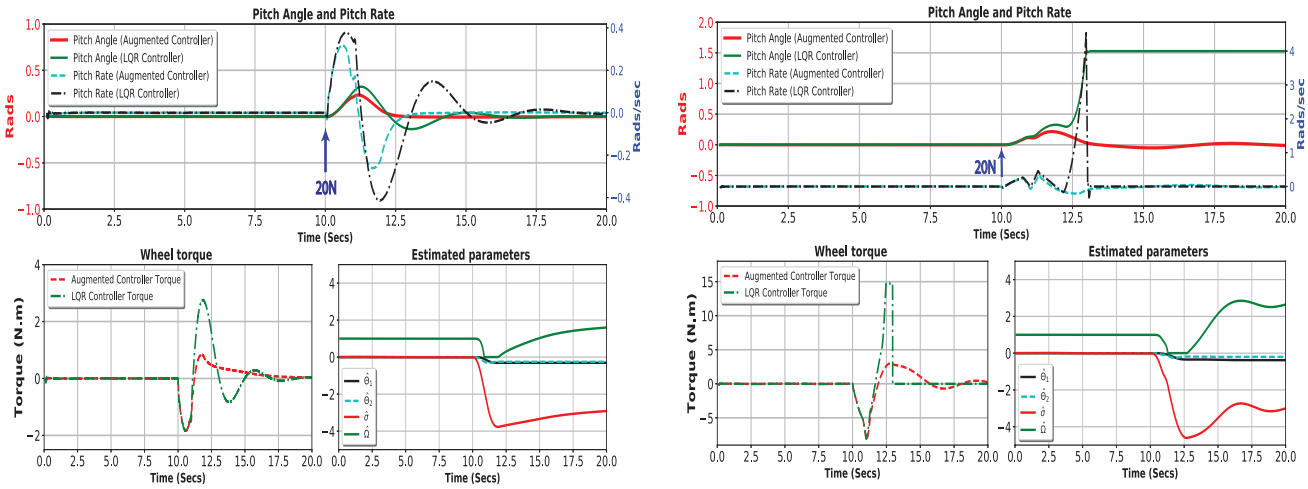

(a) Nominal case.

(b) Uncertain case, $\Delta c_r = \Delta c_l = +100\%$.

Fig. 5: Validation in simulation: Temporal evolution of pitch angle, pitch rate, wheel torque, and the estimated parameters of the augmented $\mathcal{L}_1$ adaptive controller during a push of 20N force.

odometry.

We performed a couple of experiments on the real Igor robot to compare the stability performance and energy efficiency of the two controllers in different operating conditions. The controllers have the regulation task to keep the robot balanced $\beta \approx 0$ in the presence of the external pushes. Since the real robot lacks a force sensor, we applied manual pushes repeated three times to take the average result. The first experiment is performed on a normal tiled floor with less friction between the floor and the wheels of the robot, while the second experiment is performed on a carpet floor with a better friction between the robot wheels and the ground. Also a lidar sensor of mass 1Kg is attached to the bottom of the Igor body for emulating modeling uncertainties. This extra mass is not included in the dynamic model of the robot and the LQR controller. The obtained results of these real-time experiments are displayed in Fig. 6 and further summarized quantitatively in TABLE II.

TABLE II: We use area under the curve of the pitch angle and the wheel torque to quantify the performance of the given controllers. The smaller these values are the better the corresponding controller performs in terms of settling time, overshoot, and energy consumption. The percent change indicates the percentage reduction of these areas in the case of augmented controller w.r.t the LQR.

		Simulations		
		LQR	**Augmented Controller**	**Percent Improved**
Nominal case	$\int\lvert\beta\rvert dt$	0.6157	0.3070	50.1%
	$\int\lvert\tau\rvert dt$	6.3441	3.6355	42.7%
Uncertain case	$\int\lvert\beta\rvert dt$	11.5773	0.5006	95.7%
	$\int\lvert\tau\rvert dt$	18.0505	16.2275	10.0%
		Real-time Experiments		
		LQR	**Augmented Controller**	**Percent Improved**
Tile floor	$\int\lvert\beta\rvert dt$	0.6624	0.2700	59.2%
	$\int\lvert\tau\rvert dt$	13.5188	8.8440	34.6%
Carpet floor	$\int\lvert\beta\rvert dt$	0.5160	0.3283	36.3%
	$\int\lvert\tau\rvert dt$	10.9857	10.9037	0.75%

Fig. 6a provides the evolution of the pitch angle β, pitch rate $\dot{\beta}$, wheel torque τ, and the estimated parameters of the augmented $\mathcal{L}_1$ adaptive controller versus time for the tiled floor test. It is clear that the pitch angle remains significantly smaller (about 59%) for the proposed augmented controller case compared to the LQR case. Furthermore, this enhancement in the robot stability in case of the proposed controller also comes with the benefit of a reduced wheel torque of about 34.6%. However, it is worth to note that even with model uncertainties, the LQR feedback controller successfully achieves the nominal performance by balancing the robot.

For comparison, we repeated the same tests on a carpet surface in the second experiment as shown in Fig. 6b. It is noted that with similar pushes, the deviation of the pitch angle from the given reference point stays smaller for the proposed augmented controller than for the LQR. However, this difference is reduced from 59.2% to 36.3% in the case of carpet floor. Furthermore, due to high friction between the carpet floor and the robot wheels, both controllers give the similar torque profiles to keep the robot balanced against the applied external pushes.

VI. Conclusion and Future Work

In this paper we proposed and implemented a linear quadratic regulator augmented with an $\mathcal{L}_1$ adaptive controller to stabilize a wheel-legged robot. It is shown through different simulations and real-time experiments that the proposed augmented controller was successfully able to compensate for the model uncertainties and external disturbances and clearly outperforms the model-based LQR controller.

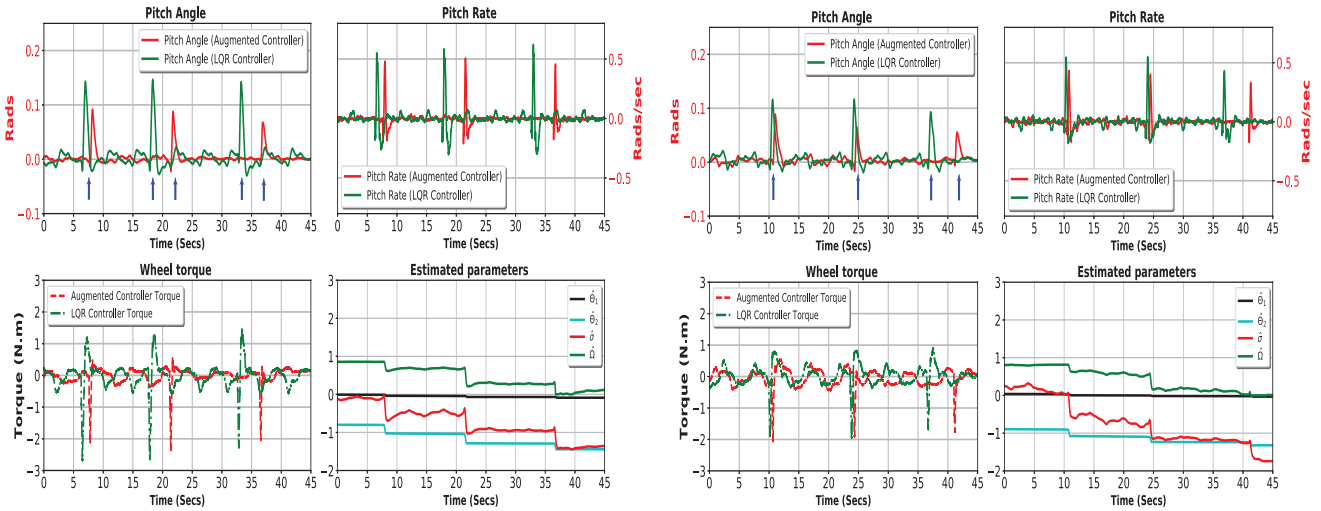

(a) Tile floor case.

(b) Carpet floor case.

Fig. 6: Validation in real-time experiments: Temporal evolution of pitch angle, pitch rate, wheel torque, and the estimated parameters of the augmented $\mathcal{L}_1$ adaptive controller subject to external pushes.

In the future work, we may focus on design and implementation of an $\mathcal{L}_1$ adaptive controller for the underactuated wheel-legged robot to control its further DoFs such as translational position, pitch angle, and the yaw angle.

REFERENCES

[1] E. Koyanagi, S. Iida, K. Kimoto, and S. Yuta, "A wheeled inverse pendulum type self-contained mobile robot and its two-dimensional trajectory control," in *2nd International symposium, Measurement and control in robotics*. JIRA, 1992, pp. 891–898.

[2] Y. Ha and S. Yuta, "Trajectory tracking control for navigation of self-contained mobile inverse pendulum," in *IEEE International Conference on Intelligent Robots and Systems (IROS)*, 1994, pp. 1875–1882.

[3] N. Shiroma, O. Matsumoto, and K. Tani, "Cooperative behavior of a mechanically unstable mobile robot for object transportation," *JSME International Journal Series C*, vol. 42, no. 4, pp. 965–973, 1999.

[4] F. Grasser, A. D'Arrigo, S. Colombi, and A. Rufer, "Joe: a mobile, inverted pendulum," *IEEE Transactions on Industrial Electronics*, vol. 49, no. 1, pp. 107–114, 2002.

[5] K. Pathak, J. Franch, and S. K. Agrawal, "Velocity control of a wheeled inverted pendulum by partial feedback linearization," in *IEEE Conference on Decision and Control (CDC)*, 2004, pp. 3962–3967.

[6] Kaustubh Pathak, Jaume Franch, and Sunil K. Agrawal, "Velocity and position control of a wheel inverted pendulum by partial feedback linearization," *IEEE Transactions on Robotics*, vol. 21, no. 3, pp. 505–513, 2005.

[7] S. Jeong and T. Takahashi, "Wheeled inverted pendulum type assistant robot: inverted mobile, standing, and sitting motions," in *IEEE International Conference on Intelligent Robots and Systems (IROS)*, 2007, pp. 1932–1937.

[8] Seonghee Jeong, and Takayuki Takahashi, "Wheeled inverted pendulum type assistant robot: design concept and mobile control," *Intelligent Service Robotics*, vol. 1, pp. 313–320, 2008.

[9] Boston Dynamics., "Introducing handle." [Online]. Available: https://www.youtube.com/watch?v=-7xvqQeoA8c

[10] X. Li, H. Zhou, S. Zhang, H. Feng, and Y. Fu, "WLR-II, a hose-less hydraulic wheel-legged robot," in *IEEE International Conference on Intelligent Robots and Systems (IROS)*, 2019, pp. 4339–4346.

[11] V. Klemm, A. Morra, C. Salzmann, F. Tschopp, K. Bodie, L. Gulich, N. Küng, D. Mannhart, C. Pfister, M. Vierneisel, F. Weber, R. Deuber, and R. Siegwart, "Ascento: A two-wheeled jumping robot," in *IEEE International Conference on Robotics and Automation (ICRA)*, 2019, pp. 7515–7521.

[12] V. Klemm, A. Morra, L. Gulich, D. Mannhart, D. Rohr, M. Kamel, Y. de Viragh, and R. Siegwart, "LQR-assisted whole-body control of a wheeled bipedal robot with kinematic loops," *IEEE Robotics and Automation Letters*, vol. 5, no. 2, pp. 3745–3752, 2020.

[13] G. Zambella, G. Lentini, M. Garabini, G. Grioli, M. G. Catalano, A. Palleschi, L. Pallottino, A. Bicchi, A. Settimi, and D. Caporale, "Dynamic whole-body control of unstable wheeled humanoid robots," *IEEE Robotics and Automation Letters*, vol. 4, no. 4, pp. 3489–3496, 2019.

[14] L. Cui, S. Wang, J. Zhang, D. Zhang, J. Lai, Y. Zheng, Z. Zhang, and Z.-P. Jiang, "Learning-based balance control of wheel-legged robots," *IEEE Robotics and Automation Letters*, vol. 6, no. 4, pp. 7667–7674, 2021.

[15] E. Li, H. Feng, H. Zhou, X. Li, Y. Zhai, S. Zhang, and Y. Fu, "Model learning for two-wheeled robot self-balance control," in *IEEE International Conference on Intelligent Robotics and Biomimetics*, 2019, pp. 1582–1587.

[16] Jian Huang, Zhi-Hong Guan, Takayuki Matsuno, Toshio Fukuda, and Kosuke Sekiyama, "Sliding-mode velocity control of mobile-wheeled inverted-pendulum systems," *IEEE Transactions on Robotics*, vol. 26, no. 4, pp. 750–758, 2010.

[17] Jian-Xin Xu, Zhao-Qin Guo, and Tong Heng Lee, "Design and implementation of integral sliding-mode control on an underactuated two-wheeled mobile robot," *IEEE Transactions on Industrial Electronics*, vol. 61, no. 7, pp. 3671–3681, 2014.

[18] M. Zafar, S. Hutchinson, and E. A. Theodorou, "Hierarchical optimization for whole-body control of wheeled inverted pendulum humanoids," in *IEEE International Conference on Robotics and Automation (ICRA)*, 2019, pp. 7535–7542.

[19] Sangtae Kim and SangJoo Kwon, "Nonlinear optimal control design for underactuated two-wheeled inverted pendulum mobile platform," *IEEE/ASME Transactions on Mechatronics*, vol. 22, no. 6, pp. 2803 – 2808, 2017.

[20] F. Raza, D. Owaki, and M. Hayashibe, "Modeling and control of a hybrid wheeled legged robot: Disturbance analysis," in *IEEE/ASME International Conference on Advanced Intelligent Mechatronics (AIM)*, 2020, pp. 466–473.

[21] F. Raza, W. Zhu, and M. Hayashibe, "Balance stability augmentation for wheel-legged biped robot through arm acceleration control," *IEEE Access*, vol. 9, pp. 54 022–54 031, 2021.

[22] N. Hovakimyan and C. Cao, *L1 Adaptive Control Theory: Guaranteed Robustness with Fast Adaptation*. Society for Industrial and Applied Mathematics, 2010.

[23] K. W. Lee and S. N. Singh, "Multi-input submarine control via L1 adaptive feedback despite uncertainties," *Journal of Systems and Control Engineering*, vol. 228, no. 5, pp. 330–347, 2014.